JOURNAL OF SPACECRAFT AND ROCKETS
Vol. 43, No. 5, September–October 2006

Catalytic and Radiative Behaviors of ZrB_2–SiC Ultrahigh Temperature Ceramic Composites

Luigi Scatteia*
Centro Italiano Ricerche Aerospaziali, 81043 Capua, Italy
Raffaele Borrelli†
University of Salerno, 84011 Baronissi, Italy
Giovanni Cosentino‡
Centro Italiano Ricerche Aerospaziali, 81043 Capua, Italy
and
Eric Bêche,§ Jean-Louis Sans,§ and Marianne Balat-Pichelin‖
Procédés Matériaux et Energie Solaire—Centre National de la Recherche Scientifique Laboratory, 66120 Font-Romeu Odeillo, France

DOI: 10.2514/1.21156

Experimental investigations of radiative properties and catalytic efficiency related to atomic oxygen recombination reaction at high temperatures were conducted on sintered ZrB_2–SiC ceramic composite designed for space applications. Total hemispherical emissivity and recombination coefficient for atomic oxygen in the range 1000–1800 K were measured. The characterization campaign was conducted using the Moyen d'Essai et de Diagnostic en Ambiance Spatiale Extrême and Moyen d'Essai Solaire d'Oxydation facilities developed at the Procédés Matériaux et Energie Solaire—Centre National de la Recherche Scientifique laboratory. Microstructural analyses prior to and after the high temperature exposure into the Moyen d'Essai Solaire d'Oxydation apparatus were also carried out using x-ray photoelectron spectroscopy, x-ray diffraction, and scanning electron microscopy. High emissivity values and low recombination coefficients were found in agreement with previous experimental studies performed on similar ceramic compounds but at lower temperatures using a different measurement technique. Samples post-analysis highlighted the oxidation-induced surface modification, and the detectable dependence of the radiative behavior upon these modifications.

Nomenclature

$D_{O,air}$	=	binary diffusion coefficient of O in air
I_{Ar}	=	intensity of argon spectral emission
I_O	=	intensity of oxygen spectral emission
i	=	total directional radiance
L	=	thickness of the recombination boundary layer of the diffusion-reaction model
n	=	refractive index
V	=	mean square velocity of atomic oxygen
T_L	=	gas temperature at the edge of the recombination boundary layer
T_S	=	surface temperature of the sample
γ	=	catalytic recombination coefficient
$\varepsilon_5^{\perp}$	=	normal spectral emissivity at 5 μm
$\varepsilon^{\cap}$	=	total hemispherical emissivity
$\varepsilon_\lambda^{\cap}$	=	spectral hemispherical emissivity
κ	=	extinction coefficient
λ	=	wavelength

Received 29 November 2005; revision received 15 March 2006; accepted for publication 16 March 2006.

*Researcher, Advanced Materials and Manufacturing Department, Via Maiorise; l.scatteia@cira.it.
†Researcher, Department of Chemistry, Via S. Allende.
‡Researcher, Advanced Materials and Manufacturing Department, Via Maiorise.
§Engineer, 7 rue du four solaire.
‖Researcher, Laboratoire Procédés, Matériaux et Energie Solaire, 7 rue du four solaire.

I. Introduction

CERAMIC compounds based on metal borides such as zirconium diboride (ZrB_2) and hafnium diboride (HfB_2) have been commonly referred as ultra high temperature ceramics (UHTCs), for their extremely high melting temperatures (respectively, around 3300 and 3500 K). UHTCs represent a class of promising materials for use in extreme applications such as sharp leading edges hot structures on the future generation of slender-shaped reentry vehicles, because of their high melting point and relatively good oxidation resistance in reentry conditions [1].

The research on this class of materials first started in the 1960s and 1970s in the context of Air Force-sponsored contracts [1]. The early works were devoted to the production of dense materials by means of pressure-assisted sintering, and to investigate the influence of a variety of additives, including carbon and silicon carbide (SiC), on the processing and oxidation resistance of Hf and Zr diborides [1]. These works showed that the addition of SiC as secondary reinforcing phase provides significant enhancements to the oxidation resistance of UHTCs. The SiC addition was also found to improve the processing by lowering sintering temperatures [2,3]. Many other studies were conducted on different compositions and their effects on the oxidation resistance performances of UHTCs, mainly in static air and ambient pressure, whereas few studies have evaluated the oxidation behavior under simulated reentry conditions [4–6].

NASA started in 1990 a research program on UHTCs, and ended up demonstrating in-flight in 1997 [7] and 2000 the use of ZrB_2 and HfB_2 sharp leading edge in the sharp hypersonic aerothermodynamic research probe ballistic experiments (SHARP-B1 and B2). Further research activities have since then been conducted in the U.S. by NASA Ames, SRI, University of Missouri Rolla, Naval Surface Warfare Center, focused on the characterization of mechanical and chemical properties [8–10] as well as on the evaluation of alternative fabrication processes such as coextrusion [11] for ZrB_2- and HfB_2–SiC.

During the 1990s, a wide range of research activity on UHTC materials was conducted in Italy, mainly by the Italian National Research Council Institute of Ceramic Materials (CNR–ISTEC). The CNR–ISTEC investigated new processing routes based on pressure-assisted sintering, on the adoption of sintering aids and secondary reinforcing phases to obtain dense bodies characterized by superior oxidation resistance and mechanical properties [12–17].

In 2000, the Italian Aerospace Research Centre (CIRA), launched the *Sharp Hot Structure* (SHS) technological project, in the frame of the Unmanned Space Vehicle (USV) National Program [18]. The project was intended to gather the national expertise owned by universities, research centers, and industries in a structured program aimed at developing the know-how needed for the manufacturing of advanced, high performance hot structures based on UHTC.

In the frame of the aforementioned project, a dedicated activity was jointly performed by CIRA with the Procédés Matériaux et Energie Solaire—Centre National de la Recherche Scientifique (PROMES–CNRS) laboratory to characterize the radiative properties and catalytic efficiency of ZrB_2-based UHTC materials.

Emissivity and catalycity represent key parameters for the eligibility of UHTC materials in hot structures manufacturing. High emissivity and low surface catalycity improve the material performance in reentry conditions, by reducing temperature gradients and thermal stresses in the structure, thus enabling the vehicle to operate under higher heat flux conditions. A reliable experimental evaluation of these parameters is required to feed aeroconvective heating computations that, in absence of experimental data, have to rely on extremely conservative theoretical values.

In addition to that, the surface catalytic behavior of the material must be fully understood in order to be able to extrapolate the structure performance in real reentry conditions from on-ground test data obtained in arc-jet facilities. Arc-jet testing provides actually the best ground-based simulation of a reentry environment. Nevertheless, surface catalycity can play a more significant role during arc-jet than it does in-flight, because a higher proportion of air molecules are dissociated in the arc-jet environment. These differences must be taken into account when designing an arc-jet experiment, and, therefore accurate catalycity experimental evaluations are required.

Many studies on radiative properties and catalytic behavior have been performed on a variety of structural and thermal protection system materials. However, few data are available for UHTC materials and their oxides. In particular, in a work of Marschall et al. [19], the catalytic atom recombination on ZrB_2–SiC and HfB_2–SiC of oxygen and nitrogen was evaluated, from room temperature up to 1000 K. In that study, the recombination coefficient was found non negligible ($\sim 5 \times 10^{-2}$), and dependant upon the surface oxidation of the material.

No data are available in literature on the surface catalytic behavior of ZrB_2-based UHTC at temperature higher than 1000 K.

In this paper, the results of an in-depth experimental investigation into the efficiency of ZrB_2–SiC compounds for heat radiation and for the recombination of atomic oxygen are reported. The study is focused on a high temperature regime (from 1000 to 1800 K) that was achieved using the solar furnaces and associated facilities Moyen d'Essai et de Diagnostic en Ambiance Spatiale Extrême (MEDIASE) and Moyen d'Essai Solaire d'Oxydation (MESOX) available at PROMES–CNRS laboratory in France [20–22]. Total hemispherical emissivity and the recombination coefficient for atomic oxygen were characterized in the range 1000–1800 K. Supportive microstructural analyses based upon x-ray microanalysis (EDS), x-ray diffraction (XRD), and scanning electron microscopy (SEM) were carried out on postcatalycity test samples in order to correlate the obtained results to the surface modifications occurring in the material during high temperature exposure.

II. Material and Experimental Measurement Methods

A. Material

Dense sintered bodies were obtained by hot isostatic pressing of ZrB_2 powders with 15 (vol%) β–SiC and 2 (vol%) $MoSi_2$ as a sintering aid to lower the temperature of the process. ZrB_2 and β–SiC raw powders were from Starck, $MoSi_2$ from Sigma–Aldrich. The process was conducted by the National Research Council Institute for Ceramic Materials located in Faenza, Italy. The obtained material has a density of 5.61 g/cm^3 which, on the basis of the rule of mixture, is higher than 99% of the theoretical density [12–17].

The material was cut and shaped in billets of 25 mm in diameter and 2 mm thickness for catalycity measurements, and 40 mm diam 2 mm thickness for emissivity experiments using electron discharge machining (EDM).

In the following, we call "pristine" samples the EDM cut billets before high temperature exposure in MESOX or MEDIASE experiments. Cross sections for microstructural investigations of the bulk material were obtained by diamond machining and by conventional metallographic polishing procedures.

B. Emissivity Measurement Method

Total hemispherical emissivity $\varepsilon^{\cap}(T)$ as a function of temperature T has been measured in the range 1000–1700 K with the MEDIASE setup developed at PROMES–CNRS laboratory [20–22], under the SOLFACE (Solar Facilities for Europe) program (6th Framework Program—European Community).

The device (Fig. 1) is composed of a vacuum chamber equipped with a hemispherical silica glass window (35 cm in diameter) for solar irradiation, a water-cooled front shield surrounding a sample holder. The specimen, in our experiments 40 mm in diameter and 2 mm thick, is heated by concentrated solar energy at the focus of the 1 MW solar furnace. On the back face of the sample, total (0.6–40 μm) and spectral directional radiance are measured by mean of a moving three-mirrors goniometer that collects the radiation emitted from the sample at different angles. The total directional radiance $i(\vartheta, T)$ is measured with a radiometer calibrated against a reference blackbody.

The total directional emissivity is then given by

$$\varepsilon(\vartheta, T) = \frac{i_S(\vartheta, T)}{i_b(T)}$$

where $i_b(T)$ is the theoretical blackbody radiation at temperature T. The same holds for spectral directional radiance $i(\lambda, \vartheta, T)$ and spectral directional emissivity $\varepsilon(\lambda, \vartheta, T)$.

The surface temperature is measured with a two-color pyrometer, developed at PROMES–CNRS laboratory [23], collecting radiation from the center of the sample. The total emissivity is readily obtained by angular integration of the directional one. Emissivity experiments have been carried out in air at 200 Pa and at 10^{-3} Pa. The uncertainty on the obtained emissivity values is evaluated as 5% for the wavelength range (0.6–40 μm) and as 10% for the spectral value (5 μm). Each emissivity evaluation test was conducted on a pristine sample.

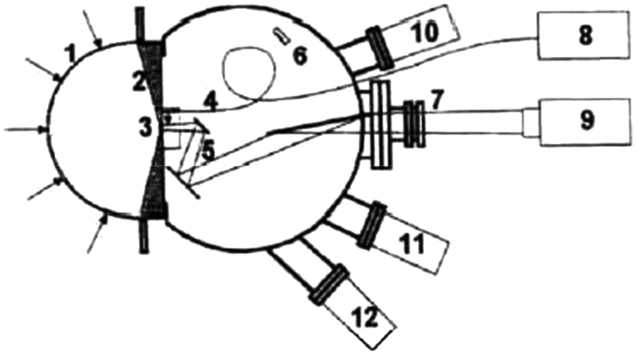

Fig. 1 MEDIASE test facility: 1) hemispherical silica window, 2) water-cooled front shield and sample holder, 3) sample, 4) optical fiber, 5) 3-mirrors goniometer, 6) quartz crystal microbalance, 7) viewport, 8) two-color pyrometer, 9) radiometer, 10) UV source position, 11) and 12) ion gun positions.

C. Catalycity Evaluation Method

The catalytic efficiency of the material for the recombination of atomic oxygen was studied by means of a direct method for the measurement of the recombination coefficient γ, defined as the ratio of the concentration of atomic oxygen which recombines on the surface to that of the total atomic oxygen impinging the surface of the sample [24]. The MESOX experimental setup, developed at PROMES–CNRS laboratory, was used for this kind of experiments.

In this apparatus the atomic oxygen recombination coefficient γ is determined by measuring the concentration gradient of atomic oxygen in proximity of the sample surface by mean of actinometry technique.

The MESOX apparatus (Fig. 2) is described in detail elsewhere [24], here we will only outline its main features. The ceramic sample (25 mm in diameter and 2 mm thickness) is put in a plasma reactor consisting of a silica tube (quartz), 50 cm length and 5 cm in diameter with CaF_2 viewports. The air plasma is generated by a 300 W microwave discharge surrounding the sample. A regulator, a gauge, and a vacuum pump allow the precise control of the total pressure during experiments. The airflow, coming from to the top of the reactor and then pumped downward, is fixed at 4 l/h. The sample is placed on a sample-holder at the center of the plasma discharge.

The reactor is positioned in such a way to let the sample be at 25 mm above the theoretical focus of the 6 kW solar furnace equipped with a variable opening shutter. Because of this shutter, the available incident concentrated solar flux can reach 5 $MW.m^{-2}$.

The relative atomic oxygen concentration in the reactor is determined by means of optical emission spectroscopy combined with actinometry. The actinometry technique allows to follow the relative atomic oxygen concentration profile along the discharge. A small amount of argon (5%) is introduced in the flow and the evolution of the ratio I_O/I_{Ar}, where I_O and I_{Ar} are the intensities of oxygen and argon emission spectral lines, respectively, is measured along the discharge zone. The transitions at 844.6 and 842.4 nm are chosen for atomic oxygen and argon, respectively. Under well-defined conditions, the ratio I_O/I_{Ar} is proportional to the oxygen concentration in a wide range of temperature and in a broad region of the reactor [24]. The spectroscopic bench is composed of an optical sampling system including a lens and a mirror, and a monochromator (spectrometer Triax 550 Jobin-Yvon) equipped with an optical multichannel analyzer (OMA). The microwave discharge is imaged by the silica lens (magnification 0.1) on the slit entrance of the monochromator. The 55 cm focal length monochromator working with a 1200 grooves/mm grating (also available 1800 and 2400 grooves/mm gratings) and a 100 μm width slit allows a spectral resolution of 0.2 nm. The dispersed light is analyzed by means of the CCD matrix (1024 × 128) of the OMA detector. Each of the 128 lines of the matrix gives information on the relative atomic oxygen concentration at different distances from the surface of the sample with a spatial resolution around 270 μm. A spectral analysis over the 128 lines is performed very quickly after the solar radiation breaking. The total duration of a scan is 200 ms. Therefore, all the spectral and spatial needed informations are taken simultaneously allowing a good accuracy.

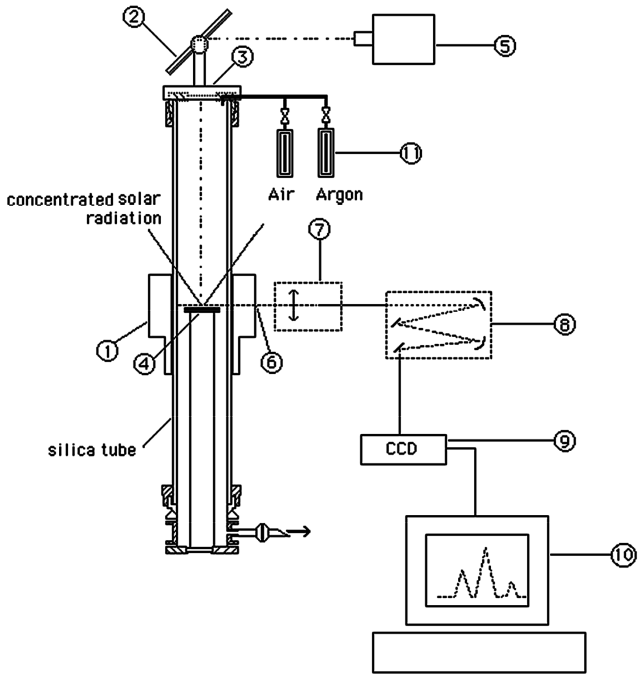

Fig. 2 MESOX setup for optical emission spectroscopy measurements : 1-waveguide, 2-mirror, 3-viewport, 4-sample, 5-pyrometer, 6-aiming slit, 7-lens, 8-spectrometer, 9-CCD-3000, 10-computer, 11-mass flowmeters.

Once the concentration profile of the atomic oxygen has been measured, the recombination coefficient is obtained according to the relation

$$\gamma = \left(\frac{\frac{I_O}{I_{Ar}}|_{x=L}}{\frac{I_O}{I_{Ar}}|_{x=0}} \cdot \frac{T_s}{T_L} - 1 \right) \frac{4D_{O,air}}{VL}$$

where $D_{O,air}$ is the binary diffusion coefficient of O in air calculated for each gas temperature by the Chapman–Enskog theory, V the mean square velocity of atomic oxygen calculated by the gas kinetic theory, L the thickness of the recombination boundary layer which enters in the diffusion-reaction model and which is measured experimentally, $(I_O/I_{Ar})_{x=L}$ and $(I_O/I_{Ar})_{x=0}$ are the measured intensities ratios at distance L from the surface and on the surface, respectively, T_s the surface temperature, and T_L the gas temperature at the edge of the layer L.

The uncertainties $\Delta\gamma/\gamma$ have been calculated taking into account the errors on I_O/I_{Ar} (10%) and L (5%) but also on the flow parameters: the diffusion coefficient $D_{O,air}$ determined using the Chapman–Enskog theory and the mean square atomic velocity V determined using the gas kinetic theory (rarefied gas). The accuracy on these two last values is due essentially to that of the gas temperature (5%), measured by optical emission spectroscopy (N_2 rotational temperature) giving a total accuracy on the recombination coefficient γ of 30%.

All the measurements were conducted on pristine samples.

D. Microstructure Characterization Methods

All specimens were examined by SEM, SEM coupled with EDS, XRD, and x-ray photoelectron spectroscopy (XPS) before and after the catalycity tests.

SEM micrographs were obtained using a S-4500 Hitachi SEM apparatus. Samples for SEM observations were prepared using argon plasma sputtering with gold electrode to obtain a sample covered with a 50 angstroms gold layer.

SEM-EDS analysis were performed using a FEI XL30 FEG environmental scanning electron microscope apparatus with energy dispersive spectroscopy x-ray detector on samples without any surface treatment, and in high vacuum (10^{-6} torr).

X-ray diffraction analyses were conducted using a PW 1820 Philips apparatus on samples without any treatment and under atmospheric pressure. XRD allows to analyze the structure of a layer approximately 20 μm thick. The aerial surface probed with this technique is about 50 mm^2.

XPS analyses were performed using a SIA Riber Cameca UHV device operating at a pressure of 10^{-6} Pa. The photoelectron emission spectra were recorded using an Al-Kα ($h\nu = 1486.6$ eV) nonmonochromatized source (600 W). The angle between the x-ray direction and the emitted electron direction was 60 deg. The analyzed area was about 25 mm^2. According to our observations on material degradation surface by electrons and ions, the ionic sputtering of the films surfaces was made by Ar^+ ion beam accelerated under 2 keV. The ion flux was fixed at about 15 $\mu A/cm^2$ for 10 min. The surface contaminant (atmospheric carbon) was removed. The kinetic energy of the photoelectrons was measured using a Riber Cameca MAC 2 spectroscopic two stages spectrometer. The analyzer resolution was

fixed at 1 eV. Spectrometer energy calibration was made using the Au 4f7/2 (83.9 ± 0.1 eV) and Cu2p3/2 (932.8 ± 0.1 eV) photoelectron lines. XPS spectra are recorded in direct N(Ec). The background signal was removed using the Shirley method [25]. The surface atomic concentrations are determined from photoelectron peaks areas (C 1s, O 1s, Si 2p, B 1s, and Zr 3d) using the atomic sensitivity factors reported by Scofield [26] or using our atomic sensitivity factors determined for reference samples and taking account the transmission function of the analyzer. The studied samples produced charging shifts (about +2 eV in binding energy). The binding energy scale was established by referencing the C 1s value of adventitious carbon (285 eV) [27,28]. The photoelectron peaks were analyzed by Gaussian/Lorentzian peak fitting. The fixed full width at half maximum (FWHM) and the fixed positions of the components are similar to those collected on our reference samples.

III. Experimental Results and Discussion

A. Emissivity Results

The two experiments performed in air at 200 Pa and at 10^{-3} Pa allow us to assess the effect of the environment on the total hemispherical emissivity of the material. The results are listed in Tables 1 and 2. As can be seen from the tables, the emissivity at 200 Pa is always higher than that at 10^{-3} Pa. This is probably because of the formation of an oxide layer that increases the emissivity in the tests at 200 Pa.

The radial dependence of the emitted radiation at 5 μm at both 200 Pa and 10^{-3} Pa was also investigated. This was done by using a bandpass filter before the radiometer in our experimental setup. Angular plots of the emissivity at 5 μm as a function of the emission angle are shown in Fig. 3. These data were used to theoretically derive additional information on the optical properties of the ZrB_2–SiC material after the tests at 10^{-3} Pa and 200 Pa. Indeed, the angular dependence of the emissivity of a bulk dielectric with a finite extinction coefficient κ can be described by the Fresnel equation [29], which depends on the refractive index n and on the extinction coefficient κ of the material. Hence, by applying a least square fitting procedure of the experimental data with the Fresnel theoretical model for bulk materials, a first estimate of these two parameters was easily obtained. Even if the bulk material model allows only to estimate mean values of the material optical properties, these values are strongly dependent upon the surface structure and can therefore be used as qualitative indexes to put in evidence surface modifications. The results of the fitting procedure are shown in Tables 3 and 4. At 10^{-3} Pa in the range of temperatures between 1000 and 1600 K, the surface of the ceramic material does not suffer dramatic changes leaving the extinction coefficient and the refraction index almost constant. On the other hand, at 200 Pa both the refractive index and the extinction coefficient decrease as temperature increases. Around 1700 K, a refractive index of about 1.4 is found. Although this is only a rough estimate, it is in line with that of silica [30], furthermore the lowering of the extinction coefficient also supports the hypothesis that the transmittance of the material is increasing. The analysis of the directional emissivity thus supports the formation of a silica-based glass layer on the material surface after exposition to an oxidizing environment. We stress that the above analysis is not meant to determine accurately the optical properties of the material but was

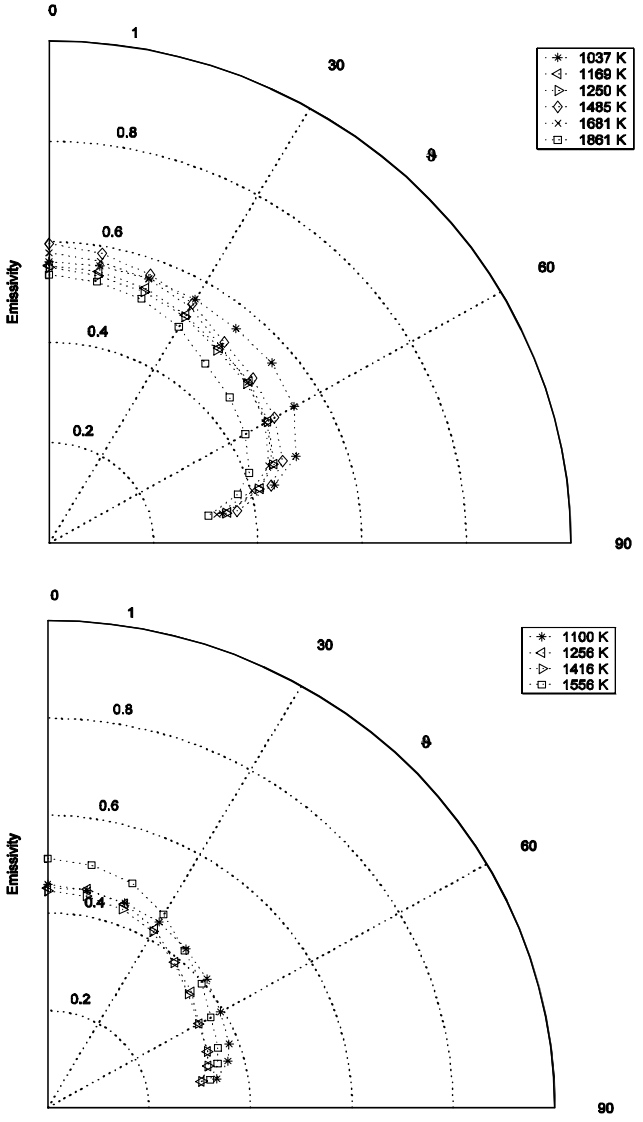

Fig. 3 Spectral directional emissivity at 5 μm at 200 Pa (upper graph) and 10^{-3} Pa (lower graph).

Table 1 Total hemispherical emissivity $\varepsilon^{\cap}$ at 200 Pa total air pressure

T (K)	$\varepsilon^{\cap}(T)$
1037	0.77
1169	0.71
1250	0.72
1319	0.73
1485	0.73
1681	0.72

Table 2 Total hemispherical emissivity $\varepsilon^{\cap}$ at 10^{-3} Pa

T (K)	$\varepsilon^{\cap}(T)$
1100	0.60
1416	0.55
1556	0.61

Table 3 Spectral ($\lambda = 5$ μm) hemispherical emissivity $\varepsilon_{\lambda}^{\cap}$, refractive index n and extinction coefficient κ of the ZrB_2–SiC as a function of temperature at 10^{-3} Pa

T (K)	$\varepsilon_{\lambda}^{\cap}(T)$	n	κ
1106	0.66	2.0	1.6
1426	0.65	1.8	1.6
1585	0.61	2.0	1.9

Table 4 Spectral ($\lambda = 5$ μm) hemispherical emissivity $\varepsilon_{\lambda}^{\cap}$, refractive index n and extinction coefficient κ of the ZrB_2–SiC as a function of temperature at 200 Pa air pressure

T (K)	$\varepsilon_{\lambda}^{\cap}(T)$	n	κ
1250	0.73	2.1	1.1
1478	0.79	1.7	0.9
1686	0.77	1.4	0.9

Table 5 Normal spectral ($\lambda = 5\ \mu$m) emissivity $\varepsilon_\lambda^\perp$ at several temperatures in the range 1000–1700 K at 200 Pa total air pressure, used for pyrometric temperature measurement with the MESOX apparatus

T (K)	$\varepsilon_\lambda^\perp(T)$
1036	0.75
1141	0.79
1250	0.78
1317	0.79
1478	0.90
1686	0.88

only performed to support the results obtained in the characterization of the high temperature behavior of the ceramic material.

Finally, the normal spectral emissivity of the samples at 5 μm as a function of the temperature at 200 Pa was also measured. This was done to obtain input emissivity values for the temperature evaluation with the monochromatic optical pyrometer used in the MESOX apparatus. The results are reported in Table 5.

B. Catalycity Results

To measure sample temperature with the optical pyrometer during catalycity experiments, a constant emissivity of 0.80 at 5 μm was chosen on the basis of the results reported in Table 5.

In Fig. 4, an example of the trend of the intensity ratio I_O/I_{Ar} as a function of the distance from the surface sample, for a ZrB_2–SiC sample heated at 1400 K is shown. We observe a constant level for the relative concentration profile until about 8 mm from the surface, followed by a progressive decrease and then, at about 2 mm from the surface, there is a change of the slope that we consider representative of the recombination process occurring on the material surface. The calculation of the thickness of the recombination boundary layer L was conducted as follows: the first eight points from the surface (2 mm) were fitted into a straight line, that was then intersected with the best fit horizontal line of the last 30 points (I_O/I_{Ar} = costant). The L value is the abscissa of this crossing point. Close to the sample surface, the ratio I_O/I_{Ar} always decreases even if the measured bulk gas and sample temperatures are the same or when the bulk gas is colder than the sample. This means that thermal effects because of the axial temperature gradients do not affect the measured atomic oxygen profiles and that these profiles are actually representative of surface chemical processes.

On Fig. 5, the atomic oxygen recombination coefficient plotted in logarithmic scale as a function of the reciprocal temperature obtained as described in Balat-Pichelin et al. [24,31], is reported from 800 up to 1800 K. The experimental values suggest the presence of a minimum γ value of 3×10^{-3} around 1000 K. After this minimum, the recombination coefficient steadily increases up to 1.7×10^{-2} at 180 K. It is evident that the function $\ln \gamma = f(1/T)$ does not follow an Arrhenius type law that predicts a linear behavior in all the temperature range, instead a change in the dependence of the curve is

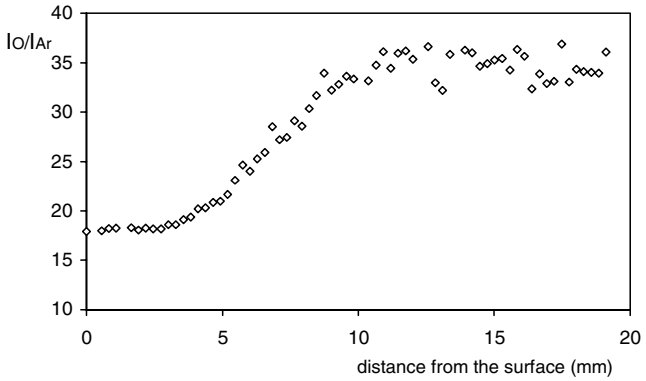

Fig. 4 Intensity ratio I_O/I_{Ar} for the ZrB_2–SiC sample heated at 1400 K under 200 Pa air plasma.

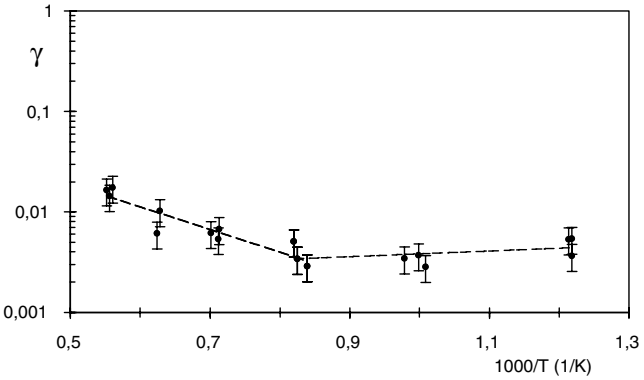

Fig. 5 Evolution of the atomic oxygen recombination coefficient on sintered ZrB_2–SiC versus reciprocal temperature.

observed around 1100–1200 K. This might suggest a change in the mechanism of atomic oxygen recombination, but further investigations are needed to assess this point.

C. Microstructural Characterization

In Fig. 6 SEM micrographs of the pristine ZrB_2–SiC material surface are reported. On these micrographs, one can notice the presence of open pores that translates into a mild surface roughness, very likely induced by the EDM machining of the billets.

SEM examination, coupled with EDS analysis, of the polished cross section of the pristine ZrB_2–SiC material is reported in Fig. 7. The analysis confirms a residual porosity lower than 1%, assesses the uniformity of the microstructure, and highlights the presence of ZrO_2 as a secondary phase in the bulk.

XRD analysis performed on the polished cross section of the pristine material is reported on Fig. 8. Only two crystalline phases were detected: mainly ZrB_2 and a few β–SiC. These results are not in contradiction with the EDS analysis (that is a local analysis technique), because the overall ZrO_2 concentration is extremely low.

The SEM micrographs reported in Fig. 9 show the surface of the ZrB_2–SiC sample after the catalycity measurement. The images show a very dense and smooth layer on the surface that mainly closes the open porosity. This layer is essentially composed of alike borosilicate glass that passivates the surface as revealed by the XPS analysis performed on the same sample (as reported further on in this section).

Because (as we have already explained above) XRD analysis is performed on roughly 20 μm in the thickness of the sample, XRD results on the postcatalycity test samples, presented on Fig. 10, indicate a crystalline oxide phase composed of monoclinic ZrO_2 and a few β–SiC. No silica or borosilicate layer is revealed by XRD because of the fact that this layer is amorphous and/or very thin. However XPS analyses, whose results will be presented in the following, show the presence of this borosilicate layer that is responsible of the very low recombination coefficient obtained as reported in literature on the reaction cured glass material [32].

Table 6 shows the atomic concentration (at.%) and the photoelectron peak positions measured for C 1s, O 1s, Si $2p_{1/2,3/2}$, B 1s and Zr $3d_{3/2,5/2}$ on the pristine sample and on postcatalycity test samples. These peaks were collected on sputtered surfaces for both the samples. The atomic compositions were determined from the XPS survey spectra. C, O, Si, Zr, and B elements were detected on sputtered surfaces. The relative concentration of carbon clearly detected for the heat-treated sample is attributed to bulk species. For the pristine sample, the measured amount of Zr (12.9%) is higher in comparison with the heat-treated sample (3.4%). Mo was not detected.

The photoelectron peaks were fitted into several components that were attributed to different chemical environments. The binding energies and the FWMH values were measured for chemical environments in standard compounds (ZrO_2, ZrB_2, SiC, SiO_2, and SiO_2C_2).

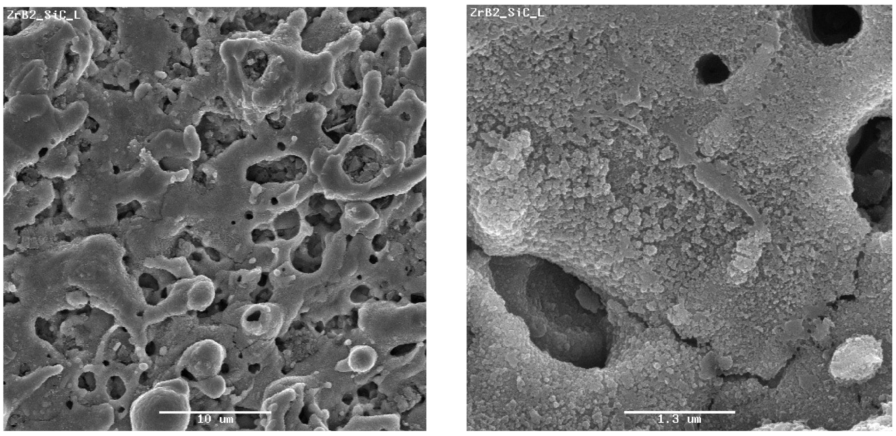

Fig. 6 SEM micrographs of the surface of the pristine ZrB_2–SiC sample.

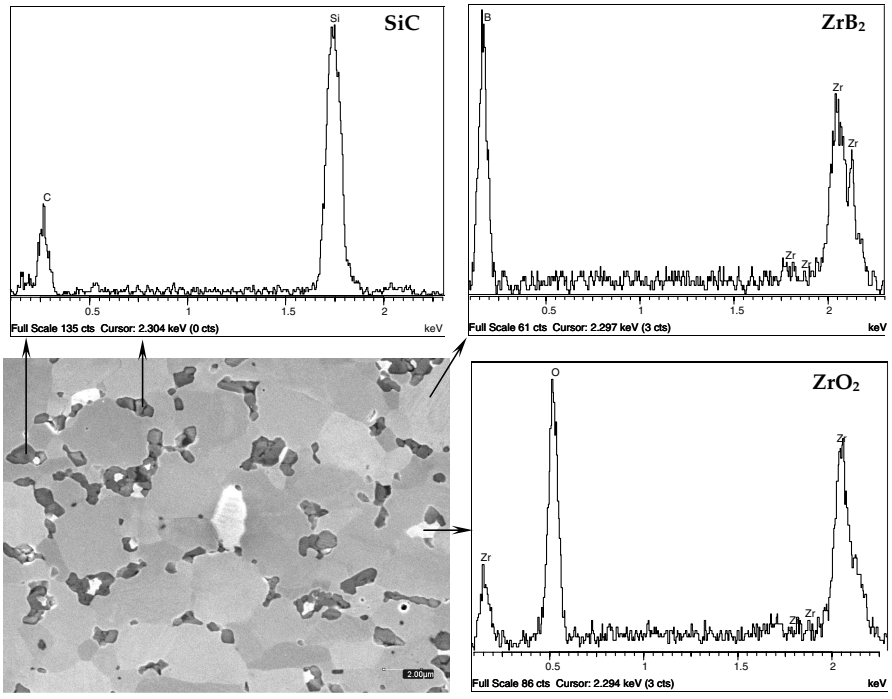

Fig. 7 SEM micrographs of a polished cross section of the pristine ZrB_2–SiC sample.

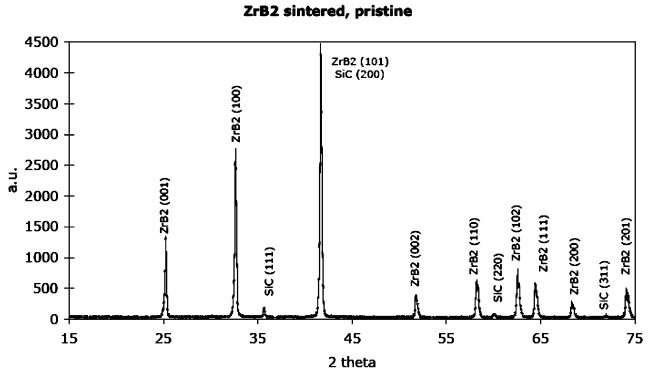

Fig. 8 XRD spectrum for the pristine ZrB_2–SiC sample.

1. C 1s Photoelectron Peak

The C 1s photoelectron peak of the pristine material can be resolved in four components (Fig. 11). The component located at 285 eV corresponds to aliphatic carbon. The other components are mainly related to carbon–oxygen bonds and carbon–silicon bonds. The component located at 286.7 and 288.6 eV are, respectively, attributed to C–O bonds and C = O bonds [27]. The component located at 283.0 eV is assigned to C–Si bonds in silicon carbide.

As can be seen in Table 6, for the heat-treated material, the percentage of the C1s peak is very low (2.6%) and it is not presented.

2. O 1s Photoelectron Peak

The results of curve fitting O 1s spectra for both samples are presented in Fig. 12. The O 1s photoelectron peak can be resolved in three components. The components located at 530.4 and 532.2 eV are, respectively, attributed to O–Zr bonds [33] and O—Si bonds [34]. The component located at 533.2 eV is characteristic of both O–C and O–B bonds [27,35]. For the pristine material, we can conclude that the O 1s photoelectron peak located at about 530.6 eV is mainly attributed to O–Zr bonds in ZrO_2 compound, whereas the O 1s photoelectron peak of the heat-treated material, located at about 532.2 eV, is mainly attributed to O–Si bonds in SiO_2 compound.

3. Si 2p Photoelectron Peak

The distribution of the silicon states resulting from the peak fitting (Si 2p spectra of both samples) is presented in Fig. 13. According to several authors [27,35,36] and our results [34], the two components located at 103.1 and 100.6 eV can be, respectively, attributed to Si–O

Table 6 Atomic concentration (at.%) and photoelectron peak positions measured for C 1s, O 1s, Si $2p_{1/2,3/2,}$, Zr $3d_{3/2,5/2}$ and B 1s for the pristine and heat-treated ZrB_2–SiC samples.

Sample	Atomic concentration (±1 at.%), Photoelectron peak position (±0.1 eV)									
	C 1s		O 1s		Si 2p		Zr 3d		B 1s	
Pristine ZrB_2–SiC	21.4	285.0	53.2	530.6	9.0	103.1	12.9	182.9	3.5	192.8
Heat-treated ZrB_2–SiC	2.6	285.0	65.2	532.4	26.8	103.1	3.4	182.9	2.0	192.8

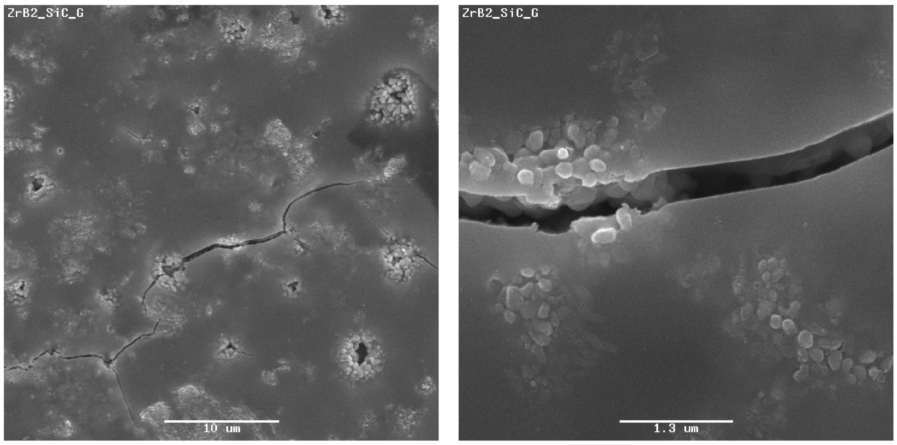

Fig. 9 SEM micrographs at two magnifications of the surface of the ZrB_2–SiC heat-treated sample after γ measurement.

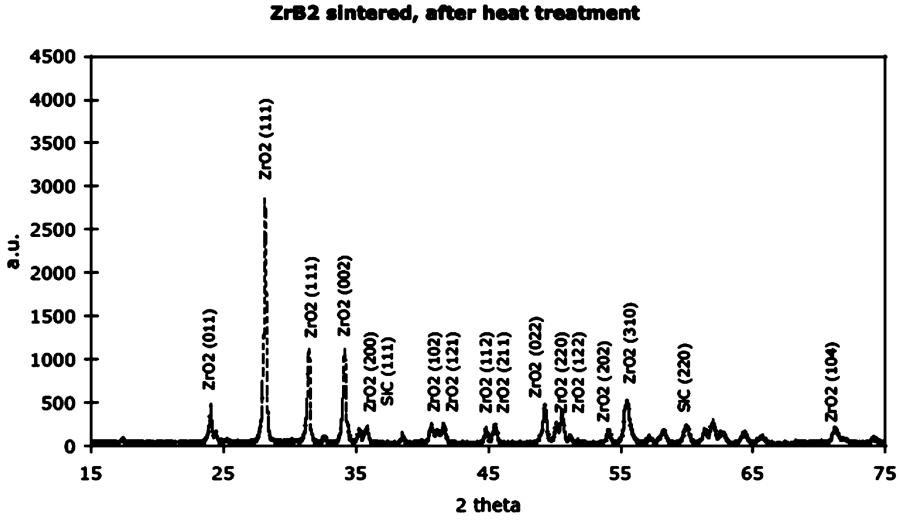

Fig. 10 XRD spectrum for the ZrB_2–SiC heat-treated sample after γ measurement.

bonds and Si–C bonds in SiO_2 and SiC compounds. The Si–C bonds were only detected for the pristine sample. The three intermediate components (101.1, 101.7, and 102.5 eV) only detected for the pristine material and that represent 3.5% were attributed to interface Si–O_xC_y compounds. Such chemical environments exist in interface compounds such as organosilicon films [37–39]. If such deconvolution is not taken into account, the peak fitting is worse. The higher the amount of silicon carbide in comparison with the amount of SiO_2, the higher the amount of these SiO_xC_y compounds [36].

4. B 1s and Zr $3d_{3/2,5/2}$ *photoelectron peaks*

Figure 14 shows the B 1s and Zr $3d_{3/2,5/2}$ photoelectron peaks and curve fitting components collected for both the samples. The components located at 182.8 ± 0.1 eV (Zr $3d_{5/2}$) and 185.0 ± 0.1 eV (Zr $3d_{3/2}$) are attributed to Zr–O bonds in a ZrO_2 compound [27,35]. The components only present for the pristine sample located at 178.7 ± 0.1 eV (Zr $3d_{5/2}$) and 181.2 ± 0.1 eV (Zr $3d_{3/2}$) are attributed to Zr–B bonds in a ZrB_2 compound. According to others studies [35–38], the small component (187.5 ± 0.1 eV) only detected for the pristine sample is attributed to B 1s photoelectron peak. This peak (included in the Zr 3d feature) was attributed to B-Zr bonds in a ZrB_2 compound. This is in good agreement with the previous results. The component located at 192.8 ± 0.1 eV (B 1s) is attributed to B–O bonds in a B_2O_3 compound [37,39].

Finally, XPS analyses allow us to conclude that the main compounds present on the surface of the pristine sample are ZrO_2 and SiO_2. Carbon oxide species, B_2O_3, SiC, and ZrB_2 in small amounts and SiO_xC_y compounds at the interface between SiO_2 and SiC (these compounds are not due to the sputtering process because they are also present for no-sputtered pristine sample) were also detected. XPS technique only probes the first few atomic layers of the material surface, and the detected composition is probably because of the EDM machining of the surface.

In the postcatalycity test sample the main compound is SiO_2, small amounts (3–4%), of ZrO_2 and B_2O_3, leading probably to the formation of a borosilicate glass on the surface, were also detected. Mo was not detected on either the pristine or the postcatalycity ZrB_2–SiC samples.

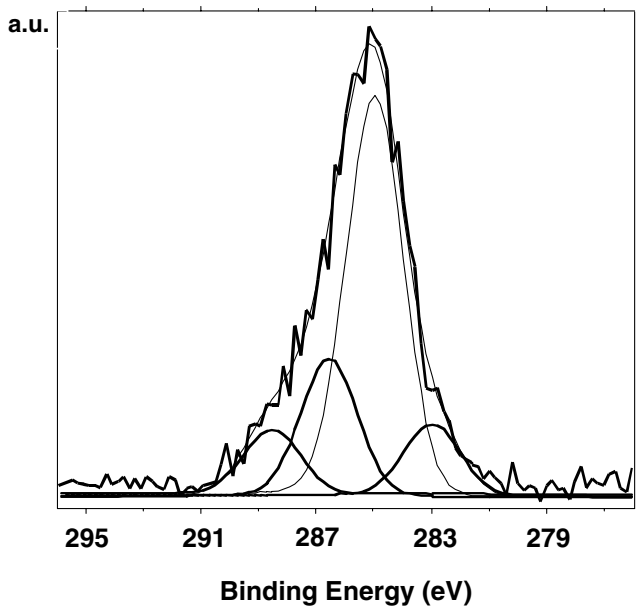

Fig. 11 C1s core-level spectrum. Curve fitting of the C 1s photoelectron peak collected for the pristine sample.

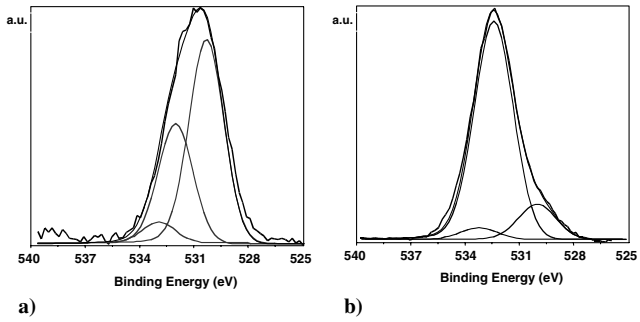

Fig. 12 O1s core-level spectra. Curve fitting of the O 1s photoelectron peaks collected for the pristine sample a) and for the heat-treated 1 b).

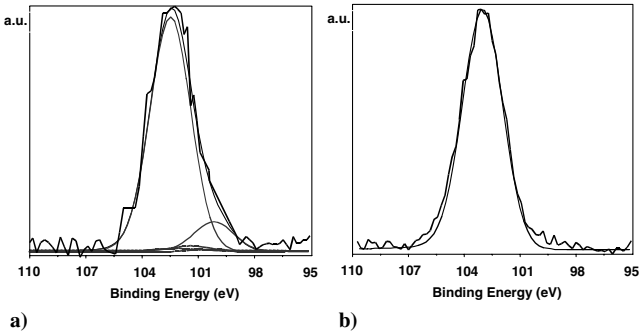

Fig. 13 Si $2p_{1/2,3/2}$ core-level spectra. Curve fitting of the Si 2p photoelectron peaks collected for the pristine sample a) and for the heat-treated 1 b).

IV. Conclusions

The ZrB_2–SiC compound characterized in our research work has already proven to be potentially suitable for the manufacturing of sharp-shaped leading edges and other kind of aerospace hot structures for hypersonic flight or reentry applications, thanks to the already assessed properties of high temperature oxidation resistance and strength retention.

The investigation performed in this research work has provided a valuable insight into the radiative and catalytic properties, crucial parameters for the selected application, and, above all, highly dependant upon the innermost microstructural nature of the examined material (and, therefore, not confidently derivable from similar materials).

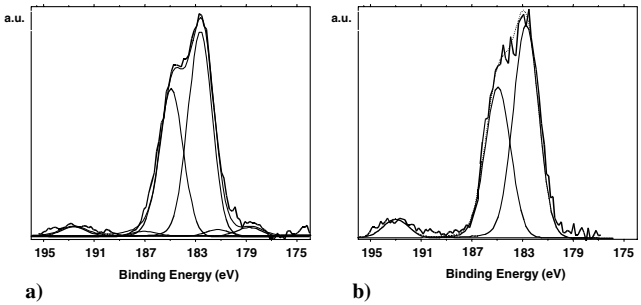

Fig. 14 B 1s and Zr $3d_{3/2,5/2}$ core-level spectra. Curve fitting of the B 1s and Zr $3d_{3/2,5/2}$ photoelectron peaks collected for the pristine sample a) and for the heat-treated 1 b).

The obtained results of the emissivity measurements have clearly highlighted the influence of the test environment upon the material emissivity. The values of total hemispherical emissivity measured under vacuum conditions are lower than the ones obtained at high pressure (200 Pa), the difference being related to the nature of the surface oxide scale formed in the second case. According to the surface analysis, the oxide scale is a silica or borosilicate glassy layer. This represents a rather promising result, because the radiative efficiency of silica-based glassy compounds is reportedly higher than that of pristine UHTCs.

For which concerns the catalytic behavior, the values obtained for the recombination coefficient with our technique are in line with those obtained at lower temperatures by Marschall et al. [19] on a similar material, manufactured for the SHARP-B1 and B2 programs in a side-arm reactor facility. Moreover the values reported here for the recombination coefficient for this material are close to those exhibited by quartz, previously obtained by Balat-Pichelin et al. [24] and by reaction cured glass from NASA [32], further confirming that the catalytic behavior of the UHTCs is mainly dictated by the surface glassy oxide scale.

The results presented in this paper are unique in the temperature range studied (800–1800 K) for such material; they allow the use in computations of a recombination coefficient value of 0.1 for temperature up to 1800 K (as a good compromise between the fully catalytic case with $\gamma = 1$ and the maximum measured value of about 2×10^{-2}). The low catalycity exhibited by the investigated UHTC composition further confirms its suitability for the intended application in the manufacturing of sharp-shaped heat shields. Work is in progress to extend the temperature range (1800–2400 K) for the measurement of the recombination coefficient.

Most interesting is the drop in the catalytic efficiency of the material around 1100–1200 K. Further investigations are ongoing in order to explain this sharp change in the catalytic behavior in that specific temperature range.

Acknowledgments

This study was realized under the 6th Framework Programme "Integrating Activities—Transnational Access" called SOLFACE, at the PROMES–CNRS laboratory. The authors wish also to thank A. Bellosi, F. Monteverde, G. Marino, and G. Russo for their precious contribution to this research work.

References

[1] Kaufman, L., and Clougherty, E. V., "Investigation of Boride Compounds for High Temperature Applications," ManLabs RTD-TRD-N69-73497, Pt. XXXVII, Cambridge, MA, Dec. 1963.

[2] Kaufman, L., and Clougherty, E. V., "Investigation of Boride Compounds for Very High Temperature Applications," ManLabs, RTD-TRD-N63-4096, Pt. III, Cambridge, MA, March 1966.

[3] Clougherty, E. V., Kalish, D., and Peters, E. T., "Research and Development of Refractory Oxidation Resistant Diborides," U.S. Air Force AFML-TR-68-190, 1968.

[4] Kuriakose, A. K., and Margrave, J. L., "The Oxidation Kinetics of Zirconium Diboride and Zirconium Carbide at High Temperatures," *Journal of the Electrochemical Society*, Vol. 111, No. 7, 1964, pp. 827–831.

[5] Opeka, M. M., Talmy, I. G., Wuchina, E. J., Zaykoski, J. A., and Causey, S. J., "Mechanical, Thermal and Oxidation Properties of Refractory Hafnium and Zirconium Compounds," *Journal of the European Ceramic Society*, Vol. 19, No. 13, 1999, pp. 2405–2414.

[6] Levine, S. R., Opila, E. J., Halbig, M. C., Kiser, J. D., Singh, M., and Salem, J. A., "Evaluation of Ultra-High Temperature Ceramics for Aeropropulsion Use," *Journal of the European Ceramic Society*, Vol. 22, No. 14, 2002, pp. 2757–2767.

[7] Kolodziej, P., Salute, J., and Keese, D. L., "First Flight Demonstration of a Sharp Ultra High Temperature Ceramic Nosetip," NASA TM-112215, Dec. 1997.

[8] Marschall, J., Erlich, D. C., Manning, H., Duppler, W., Ellerby, D., and Gasch, M., "Microhardness and High-Velocity Impact Resistance of HfB_2/SiC and ZrB_2/SiC Composites," *Journal of Materials Science*, Vol. 39, No. 19, 2004, pp. 5959–5968.

[9] Blum, Y. D., and Kleebe, H.-J., "Chemical Reactivities of Hafnium and Its Derived Boride, Carbide and Nitride Compounds at Relatively Mild Temperatures," *Journal of Materials Science*, Vol. 39, No. 19, 2004, pp. 6023–6042.

[10] Opeka, M. M., Talmy, I. G., and Zaykoski, J. A., "Oxidation-Based Materials Selection for 2000°C+ Hypersonic Aerosurfaces: Theoretical Considerations and Historical Experience," *Journal of Materials Science*, Vol. 39, No. 19, 2004, pp. 5959–5968.

[11] Fahrenholtz, W. G., Hilmas, G. E., Chamberlain, A. L., and Zimmermann, J. W., "Processing and Characterization of ZrB_2-Based Ultra-High Temperature Monolithic and Fibrous Monolithic Ceramics," *Journal of Materials Science*, Vol. 39, No. 19, 2004, pp. 5887–5904.

[12] Bellosi, A., Monteverde, F., Dalle Fabbriche, D., and Melandri, C., "Microstructure and Properties of ZrB_2-Based Ceramics," *Journal of Materials Processing and Manufacturing Science*, Vol. 9, No. 2, 2000, pp. 156–170.

[13] Monteverde, F., Bellosi, A., and Guicciardi, S., "Processing and Properties of Zirconium Diboride-Based Composites," *Journal of the European Ceramic Society*, Vol. 22, No. 3, 2002, pp. 279–288.

[14] Monteverde, F., and Bellosi, A., "Effect of the Addition of Silicon Nitride on Sintering Behavior and Microstructure of Zirconium Diboride," *Scripta Materialia*, Vol. 46, No. 3, 2002, pp. 223–228.

[15] Monteverde, F., and Bellosi, A., "Oxidation of ZrB_2-Based Ceramics in Dry Air," *Journal of the Electrochemical Society*, Vol. 150, No. 11, 2003, pp. B552–B559.

[16] Monteverde, F., and Bellosi, A., "Microstructure and Properties of an HfB_2–SiC Composite for Ultra-High Temperature Applications," *Advanced Engineering Materials*, Vol. 6, No. 5, 2004, pp. 331–336.

[17] Monteverde, F., Guicciardi, S., and Bellosi, A., "Advances in Microstructure and Mechanical Properties of Zirconium Diboride-Based Ceramics," *Materials Science and Engineering A*, Vol. 346, No. 1, 2003, pp. 310–319.

[18] Russo, G., and Marino, G., "The USV Program & UHTC Development," *Proceedings of the 4th European Workshop on Thermal Protection Systems for Space Vehicles*, edited by A. Wilson, European Space Agency, Paris, April 2003, pp. 157–163.

[19] Marschall, J., Chamberlain, A., Crunkleton, D., and Rogers, B., "Catalytic Atom Recombination on ZrB_2/SiC and HfB_2/SiC Ultra-High Temperature Ceramic Composites," *Journal of Spacecraft and Rockets*, Vol. 41, No. 4, 2004, pp. 576–581.

[20] Balat-Pichelin, M., Hernandez, D., Olalde, G., Rivoire, B., and Robert, J. F., "Concentrated Solar Energy as a Diagnostic Tool to Study Materials Under Extreme Conditions," *Journal of Solar Energy Engineering*, Vol. 124, No. 3, 2002, pp. 215–222.

[21] Paulmier, T., Balat-Pichelin, M., Le Quéau, D., Berjoan, R., and Robert, J. F., "Physico-Chemical Behaviour of Carbon Materials Under High Temperature and Ion Irradiation," *Applied Surface Science*, Vol. 180, No. 3–4, 2001, pp. 227–245.

[22] Paulmier, T., Balat-Pichelin, M., and Le Quéau, D., "Structural Modifications of Carbon–Carbon Composites Under High Temperature and Ion Irradiation," *Applied Surface Science*, Vol. 243, No. 1–4, 2005, pp. 376–393.

[23] Hernandez, D., Olalde, G., Beck, A., and Milcent, E., "Bicolor Pyroreflectometer Using an Optical Fiber Probe," *Review of Scientific Instruments*, Vol. 66, No. 12, 1995, pp. 5548–5551.

[24] Balat-Pichelin, M., Badie, J. M., Berjoan, R., and Boubert, P., "Recombination Coefficient of Atomic Oxygen on Ceramic Materials Under Earth Re-Entry Conditions by Optical Emission Spectroscopy," *Chemical Physics*, Vol. 291, No. 2, 2003, pp. 181–194.

[25] Shirley, D. A., "High-Resolution X-Ray Photoemission Spectrum of the Valence Bands of Gold," *Physical Review B*, Vol. 5, No. 12, 1972, pp. 4709–4714.

[26] Scofield, J. H., "Hartree–Slater Subshell Photoionization Cross-Sections at 1254 and 1487 eV," *Journal of Electron Spectroscopy and Related Phenomena*, Vol. 8, No. 2, 1976, pp. 129–137.

[27] Briggs, D., and Seah, M. P., *Practical Surface Analysis, Auger and X-Ray Photoelectron Spectroscopy*, J. Wiley & Sons, New-York, 1990.

[28] Smith, G. C., "Evaluation of a Simple Correction for the Hydrocarbon Contamination Layer in Quantitative Surface Analysis by XPS," *Journal of Electron Spectroscopy and Related Phenomena*, Vol. 148, No. 1, 2005, pp. 21–28.

[29] Robert Siegel, and John Howell, *Thermal Radiation Heat Transfer*, 4th ed., Taylor & Francis, New York, 2002.

[30] Wolfe, W. L., *Handbook of Optics*, edited by W. G. Driscoll and W. Vaughan, McGraw–Hill, New York, 1978, Chap. 7.

[31] Balat, M. J. H., Czerniak, M., and Badie, J. M., "Ceramic Catalysis Evaluation at High Temperature Using Thermal and Chemical Approaches," *Journal of Spacecraft and Rockets*, Vol. 36, No. 2, 1999, pp. 273–279.

[32] Rakich, J. V., Stewart, D. A., and Lanfranco, M. J., "Catalytic Efficiency of the Space Shuttle Heat Shield," *Progress in Astronautics and Aeronautics*, Vol. 85, 1983, pp. 97–122.

[33] Dzhurinskii, B. F., Gati, D., Sergushin, N. P., Nefedov, V. I., and Salyn, YA. V., "The X-Ray Electronic Studies of Oxides of Certain Element," *Russian Journal of Inorganic Chemistry*, Vol. 20, No. 9, 1975, pp. 2307–2314.

[34] Bêche, E., Berjoan, R., Roger, J. A., Dupuy, C. H. S., "XPS and AES Analysis of SiO Thin Film: A Comparative Study with Si, SiO_2 and Si/SiO_2 Interlayer," *Journal of High Temperature Chemical Processes*, Vol. 3, No. 5, 1994, pp. 555–565.

[35] Monticelli, C., Zucchi, F., Pagnoni, A., and Dal Colle, M., "Corrosion of a Zirconium Diboride/Silicon Carbide Composite in Acqueous Solution," *Electrochimica Acta*, Vol. 50, No. 16–17, 2005, pp. 3461–3469.

[36] Avila, A., Montero, I., Galan, L., Ripalda, J. M., and Levy, R., "Behaviour of Oxygen-Doped SiC Thin Films: An X-Ray Photoelectron Spectroscopy Study," *Journal of Applied Physics*, Vol. 89, No. 1, 2001, pp. 212–216.

[37] Berjoan, R., Bêche, E., Pérarnau, D., Roualdes, S., and Durand, J., "XPS and XPS Valence Band Characterizations of Amorphous or Polymeric Silicon Based Thin Films Prepared by PACVD from Organosilicon Monomers," *Journal de Physique IV*, Vol. 9, 1999, pp. 1059–1068.

[38] Roualdes, S., Van Der Lee, A., Berjoan, R., Sanchez, J., and Durand, J., "Materials, Interfaces and Electrochemical Phenomena: Gas Separation Properties of Organosilicon Plasma Polymerized Membranes," *AIChE Journal*, Vol. 45, No. 7, 1999, p. 1566.

[39] Roualdes, S., Hovnanian, N., Van Der Lee, A., Berjoan, R., and Durand, J., "Organic/Inorganic Thin Films Deposited from Diethoxydimethylsilane by Plasma Enhanced Chemical Vapor Deposition," *Journal of Non-Crystalline Solids*, Vol. 248, 1999, pp. 235–246.

A. Ketsdever
Associate Editor